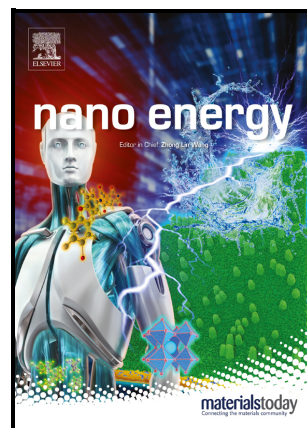


Spatial mapping of potassium diffusion and intercalation in few-layer graphene studied by ultra-high vacuum micro-Raman spectroscopy

Dario Marchiani, Nuria Jimenez Arevalo, Marco Sbroscia, Claudia Cardoso, Deborah Prezzi, Carlo Mariani, Maria Grazia Betti, Riccardo Frisenda



PII: S2211-2855(25)00633-0

DOI: <https://doi.org/10.1016/j.nanoen.2025.111274>

Reference: NANOEN111274

To appear in: *Nano Energy*

Received date: 26 July 2024

Revised date: 16 May 2025

Accepted date: 22 June 2025

Please cite this article as: Dario Marchiani, Nuria Jimenez Arevalo, Marco Sbroscia, Claudia Cardoso, Deborah Prezzi, Carlo Mariani, Maria Grazia Betti and Riccardo Frisenda, Spatial mapping of potassium diffusion and intercalation in few-layer graphene studied by ultra-high vacuum micro-Raman spectroscopy, *Nano Energy*, (2025) doi:<https://doi.org/10.1016/j.nanoen.2025.111274>

This is a PDF file of an article that has undergone enhancements after acceptance, such as the addition of a cover page and metadata, and formatting for readability, but it is not yet the definitive version of record. This version will undergo additional copyediting, typesetting and review before it is published in its final form, but we are providing this version to give early visibility of the article. Please note that, during the production process, errors may be discovered which could affect the content, and all legal disclaimers that apply to the journal pertain.

Spatial mapping of potassium diffusion and intercalation in few-layer graphene studied by ultra-high vacuum micro-Raman spectroscopy

Dario Marchiani¹, Nuria Jimenez Arevalo¹, Marco Sbroscia¹, Claudia Cardoso², Deborah Prezzi², Carlo Mariani¹, Maria Grazia Betti¹, and Riccardo Frisenda^{1,*}

¹ Physics Department, Sapienza University of Rome, Piazzale Aldo Moro 5, 00185 Rome, Italy

² S3 Center, Istituto Nanoscienze, CNR, Via Campi 213/a, Modena, Italy

*E-mail: riccardo.frisenda@uniroma1.it

ABSTRACT: Graphite, with its van der Waals layered structure, can accommodate a diverse array of intercalant species within its layers. Alkali metals (AMs), a family of donor intercalants, play a pivotal role in technological advancements, notably in lithium-ion batteries. Owing to its structural simplicity and the feasibility of producing high-quality single crystals spanning areas up to hundreds of micrometers squared, few-layer (FL) graphene serves as an exemplary system for investigating the dynamics of AM adsorption and intercalation. This study focuses on the deposition of potassium atoms in ultra-high vacuum onto mechanically exfoliated four- to five-layer FL and multilayer (ML) graphene. Employing spatially resolved Raman spectroscopy, we examine the impact of potassium adsorption, diffusion, and intercalation. Our findings reveal intricate potassium intake spatial patterns in FL graphene. The distinct spatial inhomogeneities of FL graphene are not observed in ML graphene. Density functional theory calculations also confirmed a complex scenario where both charging and steric hindrance introduce local strain in the graphene layers. Furthermore, charge donation from potassium atoms both to adjacent graphene layers and to more distant layers not adjacent to potassium atoms suggest a modification of the structural and vibrational properties of graphene consistent with the Raman experiments. The detection of intercalation fronts and domains with constant charging, and thus constant potassium densities, underscores the complex and collective nature of the potassium diffusion and intercalation in FL graphene, offering valuable insights for potential applications in energy storage systems.

KEYWORDS: graphite intercalation compounds, graphene, Raman spectroscopy, charge transfer, strain, DFT.

1. Introduction

Graphite intercalation compounds (GICs) form an important class of materials first observed almost two centuries ago [1]. Thanks to its layered structure based on van der Waals forces, graphite can host a large

variety of intercalant species between its layers [2-4]. Among others, alkali metals (AMs) are a class of donor intercalants with significant technological applications, e.g. in energy storage in lithium-ion batteries [5-7]. Potassium is an abundant and inexpensive AM that has been proposed as an alternative to the rarer and more expensive lithium for certain battery applications [8-10]. For these reasons, potassium GICs are among the most studied intercalated compounds both experimentally and theoretically. Nevertheless, the majority of literature focused so far on bulk graphitic systems in thermodynamical structural equilibrium (i.e. stoichiometric compounds such as KC_{24} or KC_8) [6,11], whereas the dynamics and diffusion of intercalant species in graphite in intermediate phases is still poorly understood and only a few recent experimental reports can be found about this topic [12-16].

An interesting effect that takes place in GICs is the periodical spacing in the stacking direction between the intercalants, as shown by X-ray and electron diffraction measurements of intercalated graphite [17]. Thus, thermodynamically stable phases of these systems are commonly referred to using the stage number n , which is the number of graphene sheets found between two intercalant layers. One open question about GICs is how their stage number changes, for example from 4 to 3 or equivalently from KC_{48} to KC_{36} . The Daumas-Herold (DH) model explains this change supposing that the intercalants do not fill up the whole space (gallery) between two graphene sheets, but form local domains [18]. Thus to change the stage number, the intercalants do not need to move out of a gallery to enter another one, but they can slide within the same gallery to form a different local stage. However, most of the experiments assess the global behavior and not the microscopic level, therefore an exhaustive answer to this question is still missing.

The isolation of graphene in 2004 by Geim and Novoselov sparked a revolution in materials science and nanoscience with the study of two-dimensional materials [19,20]. High-quality crystalline graphene can be mechanically exfoliated from graphite and further studied by different experimental techniques. Interestingly, AMs can also form stable bonds with graphene acting as donors, similarly to what happens in graphite [21-23]. Nevertheless, due to the lack of multiple layers in graphene, only adsorption of AMs can take place in such a material and no intercalation is possible, contrarily to what happens in graphite where intercalation is needed to saturate the crystal structure and reach stoichiometries such as KC_8 . Few-layer (FL) graphene is an interesting intermediate system, where both AMs intercalation and adsorption processes are expected to take place [24]. The structural simplicity and the high-quality of mechanically exfoliated FL graphene single crystals, with areas as large as hundreds of μm^2 , can be exploited to study the dynamics of these two processes. Additionally, the large ratio between defect-free basal planes versus edges in mechanically exfoliated graphene allows a more ideal diffusion and bonding of AM atoms when compared to more defective forms of graphene/graphite [25,26].

In this paper, we focus on the deposition of potassium atoms in ultra-high vacuum (UHV) onto mechanically exfoliated FL and multilayer (ML) graphene deposited on SiO_2/Si . We use spatially resolved Raman

spectroscopy as a function of potassium deposition time in UHV ambient to observe the adsorption, diffusion and intercalation process of potassium at the microscopic scale. Moreover, the charge transfer and induced strain in graphene by potassium intercalation is investigated using DFT calculations and connected to Raman measurements to better understand the physical process. Raman mapping unveils a non-trivial diffusion of potassium in FL graphene, which can be explained by the presence of energy barriers for the diffusion of adsorbed or intercalated potassium atoms and the mutual interaction between them [27-29]. Our study identifies energy barriers indirectly through spatial inhomogeneity, but explicit kinetic calculations of diffusion coefficients were not performed. Leading to a deeper understanding of GICs intercalation dynamics, our study will foster promising insight for the application in energy storage devices with better tailored properties.

2. Results and Discussions

2.1 Fabrication and characterization of transferred FL and ML graphene flakes

High-quality crystalline FL and ML graphene, defined respectively as 3-10 graphene layers and >10 graphene layers, were prepared by mechanical exfoliation from bulk graphite using Nitto tape (SPV244) and Gelpak (WF4) as described in details elsewhere [30,31]. The transmission optical microscope photograph of a transparent Gelpak stamp carrying a flake with FL and ML graphene regions is shown in Figure 1a, while Figure 1b shows an optical microscope picture of the same flake after being transferred to the SiO₂/Si substrate. After loading the sample into the ultra-high vacuum chamber, Raman spectra (532 nm excitation) were recorded for the FL and ML regions at the spots indicated by the green and red circles in Fig. 1b. Both Raman spectra shown in Figure 1c present prominent G1 (note that in literature this peak is commonly called G) and 2D peaks, which are related to the in-plane vibrations of the hexagonal lattice carbon atoms, located respectively at about 1584 cm⁻¹ and 2720 cm⁻¹. From the transmission [32] of the FL region in Fig. 1a (see also Fig. S1 of the Supporting Information) and from the 2D peak line-shape [33] in Fig. 1c we estimate the thickness of the FL region to be 4-5 layers. The D peak at 1350 cm⁻¹, a mode typically related to the presence of defects in graphene, is not detectable in our Raman spectra, confirming the high-quality, crystalline nature of the Gr sample. While the G1 peak position, common to all graphitic compounds, is not strongly affected by thickness variations, the intrinsic properties of samples from few-layer graphene to bulk graphite can be distinguished from the spectral profile of the 2D mode [34], whose line-shape evolves going from ML to FL region (see Figure 1c). Finally, the peaks observed at Raman shifts lower than 1000 cm⁻¹ are due to vibrations in the silicon substrate and are visible only in the FL region due to its lower light absorption power, while are completely attenuated in the thicker ML region.

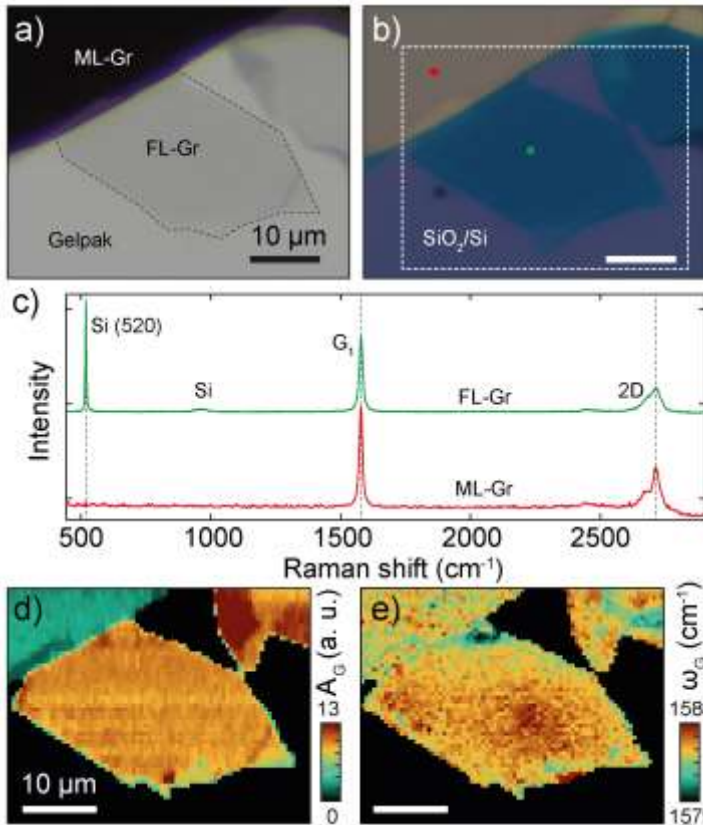


Figure 1: Few-layer and multilayer graphene fabrication and Raman characterization. a) Optical microscope photograph of the few-layer (FL) and multilayer (ML) graphene flake exfoliated onto the viscoelastic substrate Gelpak recorded in transmission illumination mode. b) Photograph of the same flake after deterministic transfer onto a 290 nm SiO₂/Si substrate taken in reflection illumination mode. c) Raman spectra of the FL and ML regions recorded with 532 nm excitation recorded in the two points highlighted by the green and red circles in panel (b). d-e) Raman maps of the G1 peak area A_G (d) and energy position ω_G (e) acquired in the region highlighted by a dashed white rectangle in panel (b).

The Raman signals were mapped by raster scanning the sample in the x-y plane with a step of 500 nm in the region highlighted in Fig. 1b by a dashed white rectangle. A full Raman spectrum was recorded for each position and each feature fitted by a Lorentzian peak, extracting the area A , the frequency ω and the width of each peak. In Figure 1d-e, the area and the position of the G1 peak are plotted as a colormap. The area of the G1 peak, which is affected by interference enhancement effects for thin layers, shows a strong dependence on the sample thickness (see also Fig. S2 of the Supporting Information). The larger area in the FL as compared to the ML helps the identification of the two regions [35,36]. On the other hand, the energy of the G1 peak does not show a strong dependence on the thickness and its value is rather homogeneous in the studied flake, except for a shallow gradient observed in the FL region, possibly due to some residual strain produced during the deterministic transfer process [37].

2.2 Raman spatial mapping of potassium intake into FL and ML graphene

Potassium atoms were deposited on Gr in the UHV preparation chamber (see Fig. S3 of the Supporting Information) in three subsequent deposition steps (10, 85 and 180 minutes) [22]. Figure 2 shows the gradual evolution of the G1 and 2D Raman peak as a function of the total potassium deposition time in two selected points of the FL and ML regions (see also Fig. S4 of the Supporting Information). Already after the first K deposition, a second peak labelled G2 appears close to G1, at around 1610 cm^{-1} Raman shifts. This peak has been reported previously in doped graphene and GICs, and it is attributed to the presence of graphene layers charged by electron donation from alkali metal adatoms or intercalated atoms [11,23,38,39]. The presence of both G1 and G2 peaks in these spectra points to an inhomogeneous doping either in the vertical direction or in-plane. In the vertical direction, the origin of the G1/G2 peaks can be explained considering that the Raman signal (acquired in a $500 \times 500\text{ nm}^2$ area) probes both charged graphene layers that are in direct contact with potassium and uncharged layers that are not in contact with potassium. In graphite, this phenomenon is known as staging, and the number of the stage n (with $n = 1, 2, 3 \dots$) refers to the following periodical arrangement: potassium layer – n graphene layers. On the other hand, in-plane inhomogeneity in ultra-thin flakes can also explain the presence of G1 and G2 peak where more (less) diluted regions are characterized by a less (more) intense G2 (a phenomenon known as in-plane staging).[40,41] In general, the observation of G1 and G2 peaks indicates that UHV sublimation of K atoms allows a gradual evolution of the system from a lower potassium/carbon stoichiometry to a larger one. The K intercalation not only leads to the appearance of a second peak, G2, but also affects the position and the line-shape of G1 peak. Previous studies on graphene doped by an applied gate voltage [42-45] show that as the Fermi level E_F moves in the graphene upper Dirac cone, the position of the G1 peak shifts to higher frequency until it reaches a maximum for highly doped samples. Furthermore, the G1 peak width narrows as E_F increases until $E_F \approx 0.1\text{ eV}$, a level corresponding to half the G1 phonon energy ($\Delta E \approx 1580\text{ cm}^{-1} \approx 0.2\text{ eV}$) [43,46]. Both these effects (G1 shift and narrowing) are visible in our spectra and especially in the FL region as compared to the ML one (Figures S5 and S6 of the Supporting Information show these spectra fitted to two Lorentzian peaks).

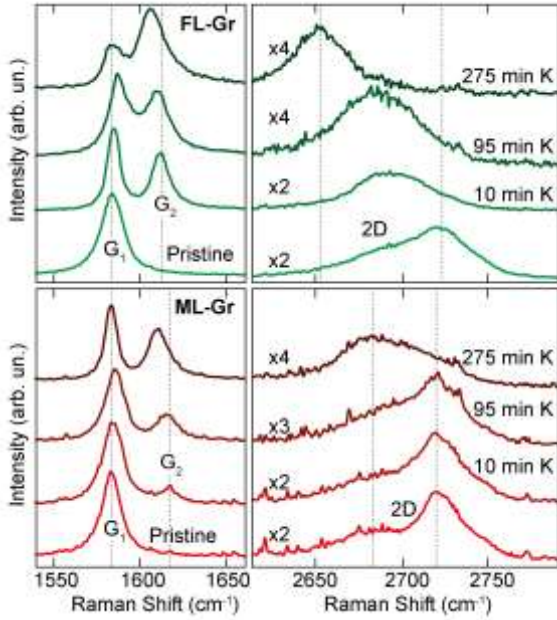


Figure 2: Raman spectra as a function of potassium intake. Raman spectra of the FL (top) and ML (bottom) regions as a function of K coverage in the G1 and 2D Raman band wavenumber range, recorded with 532 nm laser wavelength excitation. Each series of spectra is vertically stacked for clarity and the individual spectra taken in the 2D band region in the right top and bottom panels are multiplied by the factors indicated in figure (x2, x3 or x4).

In addition to the evolution of the G1 region, the spectral region of the 2D band evolves gradually as a function of K intake, as shown in Figure 2. In the FL region, we observe a redshift of the 2D band and a change in its shape and area. The line-shape of the 2D band is strongly dependent on the interaction between graphene layers [34] and, therefore, on the presence of intercalants, which can weaken the interaction between adjacent layers. Furthermore, as the 2D peak is a resonant one, it is also very sensitive to charging effects and Pauli blocking of interband transitions. In fact, the intensity of the 2D peak for graphene on Si/SiO₂ can be written as $I(2D) \approx C \left(\frac{\gamma_K}{\gamma_{ep} + 0.07|E_F|} \right)^2$ where γ_K is the rate of emission of phonons related to the 2D process and γ_{ep} is the electron-phonon scattering rate [47,48]. In our measurements the quenching of the area of the 2D peak can be explained by the electron injection from alkali metal atoms, which increases the Fermi level E_F in the Gr flake and, consequently, enhances electron-electron scattering. On the other hand, the line-shape evolution toward a single symmetric peak observed in the last deposition stages suggests a reduction of interaction between adjacent graphene layers due to the intercalation of K atoms. Similar effects on the 2D band are also observed in the ML region, although less pronounced when comparing equivalent K deposition times due to the larger number of layers. The evolution of both the G1 and G2 peaks and of the 2D band clearly indicate that potassium atoms adsorb on and intercalate in the graphene flake, donating charge to the carbon lattice. Apart from the Raman bands just discussed, no additional peaks appear in our Raman spectra, for example in the D peak region, at any potassium evaporation step (see Fig. S5 of the Supporting Information).

To follow the spatial distribution of potassium intercalation into FL and ML graphene, we study Raman spectroscopy maps after each deposition step. In the Raman spectra of potassium-graphene compounds, the relative weight of the G2 peak compared to the G1 peak allows estimating the local potassium intake by the graphene flake. We define the variable $\theta = \frac{A_{G2}}{A_{G1}+A_{G2}}$, ranging between 0 and 1. The lowest value, 0, corresponds to the presence of the G1 peak only (pristine graphene) whereas 1 corresponds to the presence of the peak G2 only (i.e. the graphene layers are fully charged by potassium atoms). Figure 3a-c shows color maps representing the spatial distribution of θ in our sample plotted at three different deposition steps (10 minutes, 95 minutes and 275 minutes of potassium deposition times). The first map, recorded after 10 minutes of K deposition, shows that θ takes values larger than 0.1 in the full flake, indicating that the G2 peak is observed in the whole sample and that potassium atoms are bound both to the FL and ML graphene. On average, θ is larger in the FL region, assuming values between 0.4 and 0.6, than in the ML region, where θ ranges between 0.1 and 0.2. This is also evident from the histograms in Fig. 3d and is consistent with the lower number of graphene layers, since the relative weight of the G2 to G1 peaks reflects the percentage of charged layers versus uncharged ones at a certain location. Another difference between the two regions is in the spatial distribution of such values, which appear more spatially uniform in the ML region than in the FL, where sharp features separate continuous regions with larger θ from others with lower θ . By considering the homogeneity of the spatial mapping present in the pristine graphene sample (Figure 1 d-e), the spatial distribution of the spectral features observed in the FL region after K exposure can be clearly attributed to the adsorption and intercalation of K atoms, rather than to defects or intrinsic structures in FL graphene.

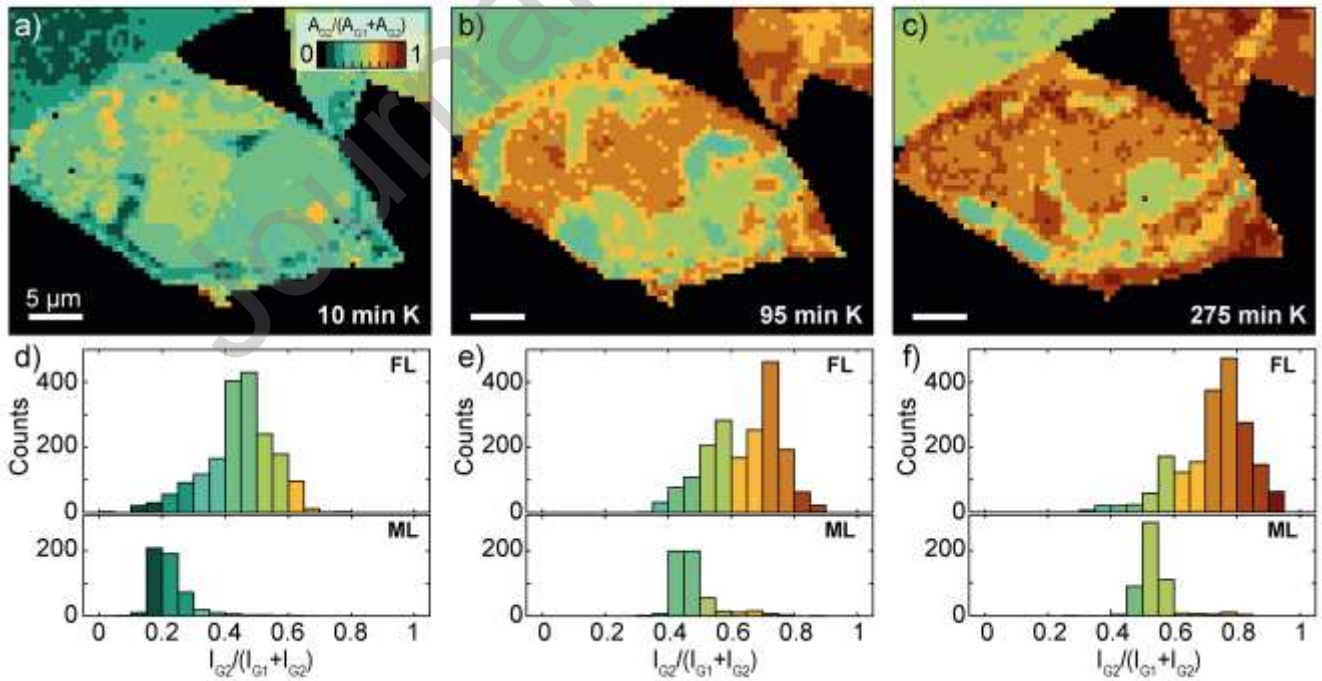


Figure 3: Spatially resolved potassium intake by Raman mapping. a-c) Raman maps of $\theta = \frac{A_{G2}}{A_{G1}+A_{G2}}$ after respectively 10, 95 and 275 minutes of K deposition. d-f) Histograms of θ constructed from the maps for the FL (top) and ML (bottom) graphene regions.

The subsequent K deposition steps, whose θ maps are shown in Figure 3b-c, show a similar behavior though the ML region remains spatially homogeneous, and the FL region clearly exhibits the formation of a large domain where the coverage reaches values as large as $\theta = 0.7$ separated from an area where $\theta=0.5$ (after 95 minutes of K deposition). Interestingly, after 275 minutes of deposition of K atoms, the large domain grows in size without the increase of the θ value, which stays around 0.7. This indicates that the local percentage of charged versus uncharged layers saturates. This behavior is also reflected in the histograms of the FL region at these two deposition steps, shown in Fig. 3e-f. The histograms present a bimodal distribution with a peak centered at $\theta = 0.5$ and another peak centered at $\theta = 0.7$. In the case of the ML region, only a single peak is observed, which gradually increases with the deposition time. These observations suggest that the intercalation of potassium atoms from the graphene edges and not from the basal planes, which would instead give a spatially homogenous signal for θ [29,49,50]. This is also reflected in the formation of domains, which indicate that the diffusion of potassium in the graphene interlayer galleries is a collective phenomenon where already intercalated K atoms need to diffuse away from an edge to allow additional K atoms to enter the gallery. A similar edge-mediated intercalation path has been reported by Zhang *et al.* for potassium electrochemically intercalating in thin MoS₂ flakes [51].

2.3 Decoupling of graphene layers induced by potassium intake

The dynamics of potassium diffusion and intercalation is clarified by the Raman mapping at different K uptakes. A careful analysis of the mapping of intercalated potassium atoms unveils a consequent decoupling of graphene layers. As shown in Figure 2, the deposition of potassium causes a dramatic change in the area and line-shape of the 2D band for both FL and ML graphene. The 2D band progressive intensity reduction upon K doping can be attributed to an enhanced electron–electron scattering rate, at increasing charge carrier density, for both adsorbed and intercalated K atoms. The 2D peak line-shape evolution can be ascribed to a mechanical separation of adjacent graphene layers (which is true only for intercalated atoms). In particular, the decoupling of graphene layers gives rise to a symmetrization of the 2D band, which evolves toward a single peak line-shape characteristic of the single-layer graphene. To study the special distribution of this phenomenon, we focus on the 2D band region of the Raman spectra mapping and fit the 2D band with two components, respectively named 2D1 and 2D2, as shown in Figure 4a. In the case of FL and ML graphene, the 2D band presents multiple components that can be well described by the 2D1 and 2D2 peaks. Conversely, a single-layer graphene presents only a single component, either 2D1 or 2D2. By defining a new variable $\varphi = \frac{I_{2D1}}{I_{2D1}+I_{2D2}}$ we can quantify the relative weights of the two 2D band components and discriminate a FL or ML Raman peak behavior from a 1L one. In fact, φ is equal to 0 (or 1) when only a single component is present in the 2D band (1L) and values are in between when two components are present.

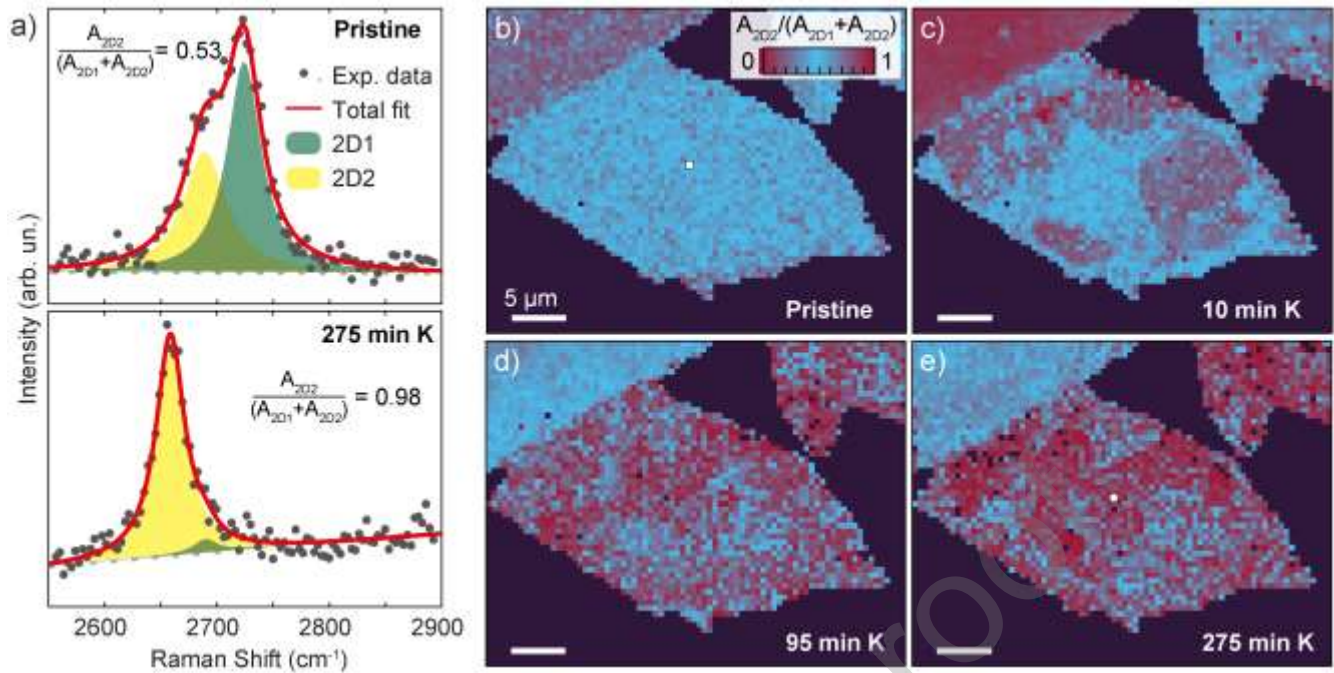


Figure 4: Decoupling of graphene layers by potassium intercalation. a) Spectra and fit to two Lorentzian peaks of the 2D band region of pristine graphene (top) and after 275 minutes of K deposition (bottom) recorded at the positions marked in panels b and e. b-e) Raman maps of $\varphi = \frac{I_{2D2}}{I_{2D1} + I_{2D2}}$ in the pristine case and after respectively 10, 95 and 275 minutes of K deposition. The white circle in panel (b) and the white square in panel (e) indicate the locations where the Raman spectra in Fig. 4a have been recorded.

Figure 4b-e shows the spatial maps of φ extracted from the fits in the case of pristine graphene (Fig. 4b) and at increasing potassium dose (Fig. 4c-e). In the pristine case, the FL region assumes a uniform light blue color, indicative of $\varphi \approx 0.5$ due to the presence of two components in the 2D band of approximately equal weight (see also the fit shown in the top panel of Fig. 4a). For increasing potassium density, the FL region goes from light blue to red color, which corresponds to φ closer to 0 or 1 and indicates the presence of a single 2D peak, as expected for a monolayer or for multiple non-interacting stacked graphene layers. This change in behavior of the 2D band suggests that the initially interacting AB-stacked graphene layers become decoupled due to the presence of potassium in the interlayer galleries. The intercalation of potassium atoms is the driving force behind this effect and thus the φ variable allows the spatial study of the intercalation process.

Interestingly, as already discussed in the case of G1 and G2 spatial maps, the φ maps also display the formation of domains for the intermediate density of potassium, indicating that potassium atoms penetrate in the graphene interlayer galleries from the edges or from few local regions and do not penetrate homogeneously from the basal planes. In fact, a potassium intercalation dynamics from the basal plane would result in a spatially homogenous signal from both φ and θ , which we do not observe. A more spatially homogeneous

signal from φ is only observed in the final potassium deposition (Fig. 4e), where most of the graphene planes are decoupled and the 2D band is composed of one peak only, as shown in the bottom panel of Fig. 4a.

The collective intercalation of alkali metal atoms in two-dimensional systems, which results in the formation of domains observed in the spatial Raman mapping, is compatible with previous experiments on the electrochemical intercalation of lithium and potassium ions into bilayer and multilayer graphene by Ji et al. who found a collective and fractal dynamics taking place in their suspended sample due to the intercalation of alkali metal ions into the bilayer gallery [40]. Overall our results show the formation of domains, which better agrees with the inhomogeneous, domain-based distribution proposed by the DH model and by more recent theoretical results[52,53] than with the homogeneous staging model proposed by Rudorff and Hoffmann (RH).

2.4 Charge and strain effects in FL and ML graphene flakes

A further step is to unveil how charging and strain effects influence the vibrational response of the FL and ML graphene flakes, at increasing density of the foreign K atoms. The spatial evolution of the G1 and G2 peaks energy as a function of K dose is reported in Figure 4, after 10, 95 and 275 minutes of K deposition. Following the evolution of the Raman shift of the G1 peak, we can deduce the areas of the C mesh not in contact with K atoms (Fig. 5a-c). On the other side, the effects of K adatoms in contact with the Gr layers can be unraveled by the evolution of the frequency of G2 (Fig. 5d-f). After the first deposition step (10 minutes of K), we observe in the FL the appearance of regions where the G1 peak downshifts with respect to the pristine value of about -2 cm^{-1} and regions where the G1 peak upshifts of about 2 cm^{-1} (see also Figure S9 of the Supporting Information). Conversely, in the whole ML flake the G1 peak upshifts of about 1 cm^{-1} .

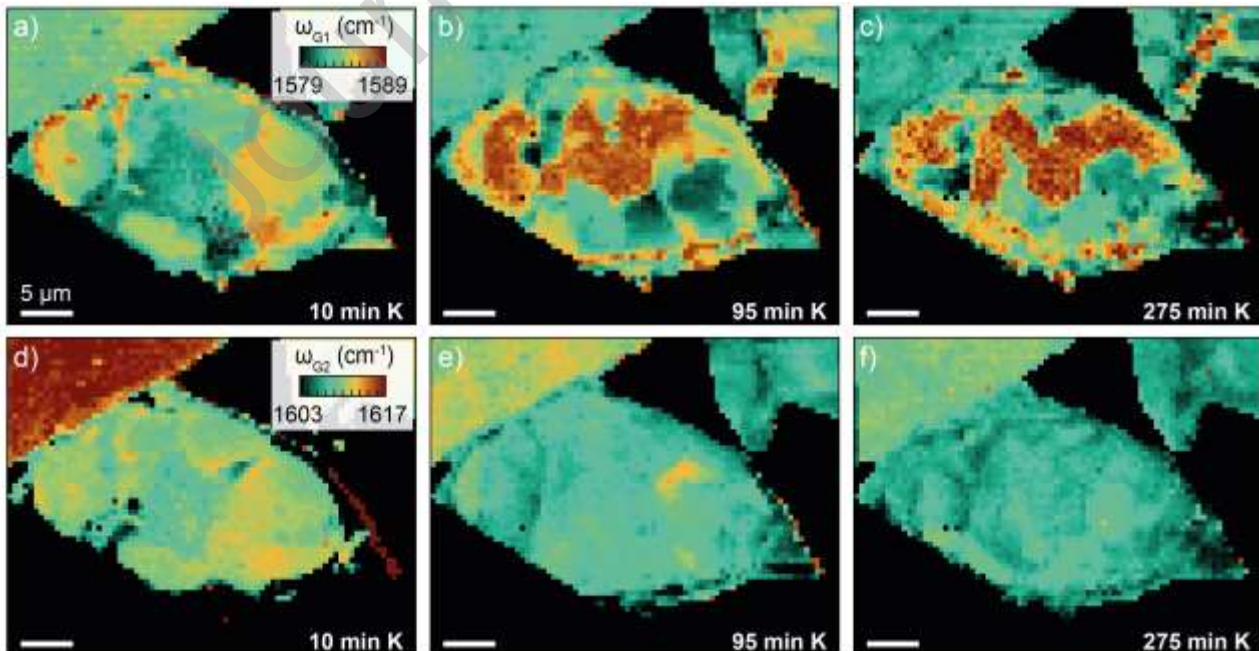


Figure 5: Charging and strain effects in few-layer and multilayer graphene studied by Raman

mapping. a-f) Raman maps of the position of G1 peak (a-c) and G2 peak (d-f) after respectively 10, 95 and 275 minutes of K deposition.

The shift of the G1 peak in graphene can be caused by both mechanical strain and charge doping [37]. In the case of biaxial strain ε , an upshift of the G1 peak is expected for compressive strain and a downshift for tensile strain with a G1 peak gauge factor, which quantifies the shift of the Raman frequency of the G1 peak as a function of biaxial strain, equal to $\frac{\partial\omega_{G1}}{\partial\varepsilon} = -55 \text{ cm}^{-1}/\%$ [54,55]. Instead, in the case of doping the G1 peak upshifts both for p-type and n-type doping with a gauge factor $\frac{\partial\omega_{G1}}{\partial n} = 7 \cdot 10^{-13} \text{ cm}^{-1}/\text{cm}^{-2}$ [46]. The total shift of the G1 peak can then be calculated according to the formula $\Delta\omega_{G1}(\Delta\varepsilon, \Delta n) = \frac{\partial\omega_{G1}}{\partial\varepsilon} \Delta\varepsilon + \frac{\partial\omega_{G1}}{\partial n} |\Delta n|$, which allows to calculate the shift of the G1 Raman band for a finite amount of strain $\Delta\varepsilon$ and charge Δn [37]. Given the observed ambipolar nature of the G1 peak shift, we ascribe the observed up- and downshifts mostly to strain. This would indicate that for FL graphene some regions undergo compression while other regions undergo tension due to the presence of potassium. Interestingly, in the case of larger potassium doses (95 and 275 deposition minutes), the G1 peak energy spatial maps are positively correlated with the width of the G1 peak (see Figure S10 of the Supporting Information), i.e. a larger G1 positive energy shift corresponds also to larger full width at half maximum. Such a larger peak width indicates a larger local inhomogeneity, which can be due to the formation of pleats or locally strained regions in the graphene layers due to the presence of potassium [53,56].

In the case of ML graphene the first step of deposition causes an overall compression of the lattice. Interestingly in this first phase the position of the G1 peak is spatially anticorrelated with the presence of potassium deduced from the maps of θ in Fig. 3a. This situation is reversed for the second and third steps of K deposition where the G peak position maps are spatially positively correlated with the presence of potassium (see Fig. 3b-c). Also, in the second and third deposition steps the overall upshifts are larger than the first step while the downshifts are comparable with the first deposition step. Such an increase in upshift could be due to additional doping from potassium atoms, which shift the G1 peak position to larger Raman shifts.

On the other hand, the maps of the G2 peak position reported in Fig. 5d-f show a more spatially homogenous behavior, being on average upshifted of approximately 25 cm^{-1} from the position of the pristine G1 peak due to charging effects and the breakdown of the adiabatic Born-Oppenheimer approximation [57]. This can be described by the formula $\hbar\Delta\omega = \alpha'|E_F|$, where $\hbar\Delta\omega$ is the change in energy of the G1 phonon mode of doped graphene with respect to the pristine case, α' is a factor relative to the electron-phonon coupling strength and E_F is the Fermi level of the doped graphene (where $E_F = 0 \text{ eV}$ corresponds to intrinsic graphene) [45,46,58]. The subsequent downshift of the G2 peak observed for higher potassium dose both in the FL and ML cases can then be ascribed to a progressive build-up of tensile strain in the charged graphene layers. This complex behavior for both the G2 and G1 Raman peaks points to an influence of potassium adsorbed and

intercalated atoms both on the graphene layer directly in contact with K atoms and on the graphene layers which are not in direct contact with the K atoms through a longer range interaction.

2.5 Charge and strain effects in K-Gr systems from DFT simulations

To better understand the effects on the charge doping and strain effects in graphene due to the presence of potassium, we performed DFT calculations for different stages and K concentrations (see Figure S12 of the Supporting Information). In Fig. 6 we show, for a stage 3 configuration, the charge transfer from K to stacked graphene computed as the difference between the charge density of the whole system, and the charge densities of pristine graphene and an isolated K atom, i.e., $\Delta\rho = \rho(\text{K-Gr}) - \rho(\text{Gr}) - \rho(\text{K})$. The charge transfer happens mainly between the K atom and the adjacent graphene sheets ($\sim 0.0184 e^-/\text{C atom}$, as estimated from the integrated charge density difference), and results in an excess charge on the p_z orbitals of graphene, which is larger on the side closer to the K atom. Interestingly, a residual excess charge is also present on the p_z orbitals of neighboring graphene sheets not in contact with the K atom ($\sim 0.006 e^-/\text{C}$, approximately one third of the charge transfer to adjacent graphene). These findings are consistent with the Raman spectra in the regions where both G1 and G2 peaks are observed and confirm that the doping inhomogeneity can take place not only in-plane, but also in the vertical direction. In fact the G2 peak is attributed to charged graphene layers, corresponding to the signal from graphene sheets adjacent to K atoms, whereas G1 corresponds to the pristine layers. The measured G2 peak presents larger variations than G1, that is mostly unperturbed with respect to pristine graphene. The small differences detected on the G1 Raman signal can then be attributed to the residual long range charge transfer to sheets not in contact with K atoms (see Figure 4).

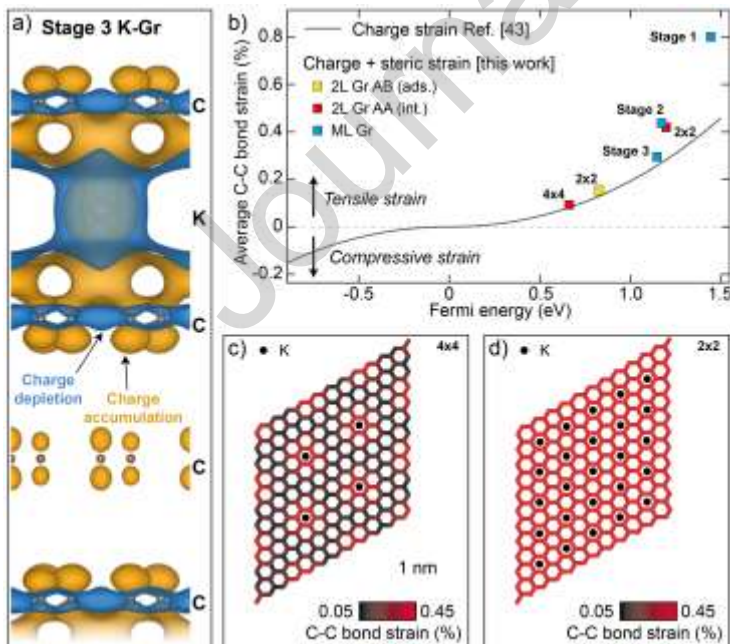


Figure 6: DFT calculations of K adsorbed onto and intercalated into bilayer and multilayer graphene, charging and strain effects. a) Differential charge density for stage 3 K-doped graphite. In orange/blue the excess/depletion of charge with respect to the isolated system. b) Calculated average C-C strain as a function of Fermi energy for bilayer (yellow and red squares for adsorbed and intercalated K, respectively) at different

K concentrations, and multilayer graphene (blue squares) at different intercalation stages. The solid black line is the strain in the case of electric field gating reproduced from Ref. [59]. c) Real space model of bilayer AA stacked graphene intercalated by K with supercell (c) 4x4 and (d) 2x2. The C-C bonds in the graphene layers are colored according to the tensile strain in the bond.

Figure 6b shows the average C-C bond strain induced in graphene by charge donation through a homogenous gate (black solid line), as reported in Ref. [59], and through adsorbed or intercalated potassium atoms (squares) for different configurations, as computed in this work (see also Figure S12 of the Supporting Information). The doping is measured by the change in the Fermi level with respect to the graphene Dirac point. For both homogeneous gate doping and explicit doping with K ions, the average strain increases with the Fermi level. However, the K doping presents a remarkably larger tensile strain for K concentrations exceeding stage 3 when compared to graphene upon homogenous charge injection. We attribute this behavior in K-Gr systems to additional steric effects from the presence of the K atoms [60,61]. To better understand the interplay between strain due to steric and charge transfer effects, we represent in Figure 6c a map of C-C bond distances in bilayer graphene intercalated by K atoms. While in a pristine graphene all the C-C bonds have the same length, after potassium adsorption/intercalation we observe local changes in the bond lengths. In particular, the C-C bonds of C atoms closer to K atoms (red color) are more strained than those from more distant C atoms (black color). If we now consider the same bilayer but increase the K concentration, going from a 4x4 to a 2x2 supercell (see Fig. 6d), the number of more strained bonds increases, resulting in a larger average strain, as illustrated by the two red squares in Figure 6b. Figure 6d shows the map of the C-C bond distances in 2x2 bilayer graphene intercalated by K atoms where a larger overall strain and a more spatially homogeneous distribution of the strain is visible. This analysis indicates that, even in more diluted potassium stages, the carbon bonds physically closer to potassium atoms can undergo a large tensile strain coming from steric effects. While calculations partially explain the non-trivial behavior of the G1 peak, they cannot capture the complexity of real samples, where additional effects have to be taken into account (e.g., defects, edges, boundaries between intercalated and non-intercalated regions) that can possibly give rise to regions with local compressive strain as observed in Figure 5. As a final note, in the GICs literature this G1 peak is normally assumed as a non-charged peak and thus independent from the presence of potassium. Our spatially resolved experiments and theory show that potassium can also influence graphene layers that are not in direct contact with those alkali atoms.

3. Conclusions

In conclusion, we investigated the sublimation of potassium atoms in ultra-high vacuum onto mechanically exfoliated four-layer and multilayer graphene. Employing spatially resolved Raman spectroscopy, we examined the impact of potassium adsorption, diffusion, and intercalation finding intricate potassium diffusion patterns in FL graphene. The detection of intercalation fronts and domains underscores the complex,

collective nature of this phenomenon and demonstrates that potassium diffusion in crystalline, low-defect FL graphene starts from the edges and not from the basal planes. Finally, thanks to DFT we better understood the effect of potassium atoms on the electronic and structural properties of graphene. In particular, in intercalated potassium staged graphite we found a charge donation from potassium atoms both to adjacent graphene layers and to more distant layers not adjacent to potassium atoms, suggesting a modification of the structural and vibrational properties of graphene consistent with the Raman experiments. Finally, we found that the effect of strain from potassium atoms comes both from charging and from steric hindrance.

Materials and Methods or Experimental

Sample fabrication. Graphene flakes were produced by micromechanical cleavage of bulk graphite and deposited on n-type Si/SiO₂ with 285 nm oxide thickness (Graphene Supermarket®). Firstly the bulk graphite crystal is pressed onto Nitto tape (SPV244) and subsequently the tape is pressed against Gelpak (WF4) to isolate thin flakes to be transferred through a deterministic transfer method onto the final substrate. Through optical inspection using an optical microscope, very large flakes (lateral size above 100 μm) were selected for the Raman mapping experiment.

Raman measurements. μ-Raman spectroscopy experiments have been carried out at the SmartLab laboratory of the Physics Department at the Sapienza, University of Rome and performed in a UHV setup using as an excitation source a single frequency ND:YVO₄ laser at 532.2 nm wavelength with a vacuum-compatible 60× objective (NA = 0.82). The power of the laser was kept below 200 μW on the sample to avoid sample damage. The system is equipped with a 50 cm focal-length monochromator with a 1200 grooves/mm grating, and the signal was detected by a back-illuminated liquid N₂-cooled Si CCD camera.

Potassium doping. Potassium doping has been carried out *in situ*, using a commercial SAES getter dispenser, after several hours of degassing at currents slightly below the current needed for potassium sublimation. The base pressure during the deposition was in the range of 10⁻¹⁰ mbar. The rate of evaporation has been estimated as (0.19±0.02) Å/minute following the procedure in Ref. [62] (see Figure S8 in the Supporting Information).

DFT calculations. Structural and doping properties of bilayer graphene and graphite upon K adsorption/intercalation were investigated from first principles by using a plane-wave pseudopotential implementation of the density functional theory (DFT), as available in the QUANTUM ESPRESSO package [63,64]. For each of the investigated systems, the atomic structure optimization was performed by using the LDA approximation for the exchange-correlation functional, together with Optimized Norm-Conserving Vanderbilt (ONCV) pseudopotentials [65], and resorting to variable-cell optimization, until pressure was lower than 0.01 Kbar, forces were less than 5×10⁻⁵ a.u, and with a convergence threshold on total energies of 10⁻⁶ a.u. For bilayer graphene, a vacuum region of about 15 Å in the non-periodic direction was introduced to prevent interaction between periodic replicas. The kinetic energy cutoff for the wave functions was set to 90 Ry; the Brillouin

zone was sampled by using a k-point distance of about 0.025 \AA^{-1} , with grids generated according to Monkhorst-Pack algorithm.

ACKNOWLEDGEMENTS

Research partially funded by the Ministero dell'Università e della Ricerca (MUR), PRIN Grants 2D-FRONTIERS (20228879FT), TUNES (2022NXLTYN) and 2D-PentaSensing (P2022HT3FF). Also partially funded by Sapienza University "Ateneo" and "Avvio alla Ricerca" Projects. The authors acknowledge the SmartLab laboratory of the Department of Physics at Sapienza University of Rome, for the all-in-UHV micro-Raman measurements, and the CINECA award under the ISCRA initiative for the availability of high-performance computing resources and support.

COMPETING INTERESTS

The authors declare no competing financial interests.

FUNDING

Ministero dell'Università e della Ricerca (MUR): PRIN Grants 2D-FRONTIERS (20228879FT) and 2D-PentaSensing (P2022HT3FF), TUNES (2022NXLTYN).

Sapienza University of Rome: Ateneo funds "Progetti di Ricerca Medi" 2022, 2021, 2023.

REFERENCES

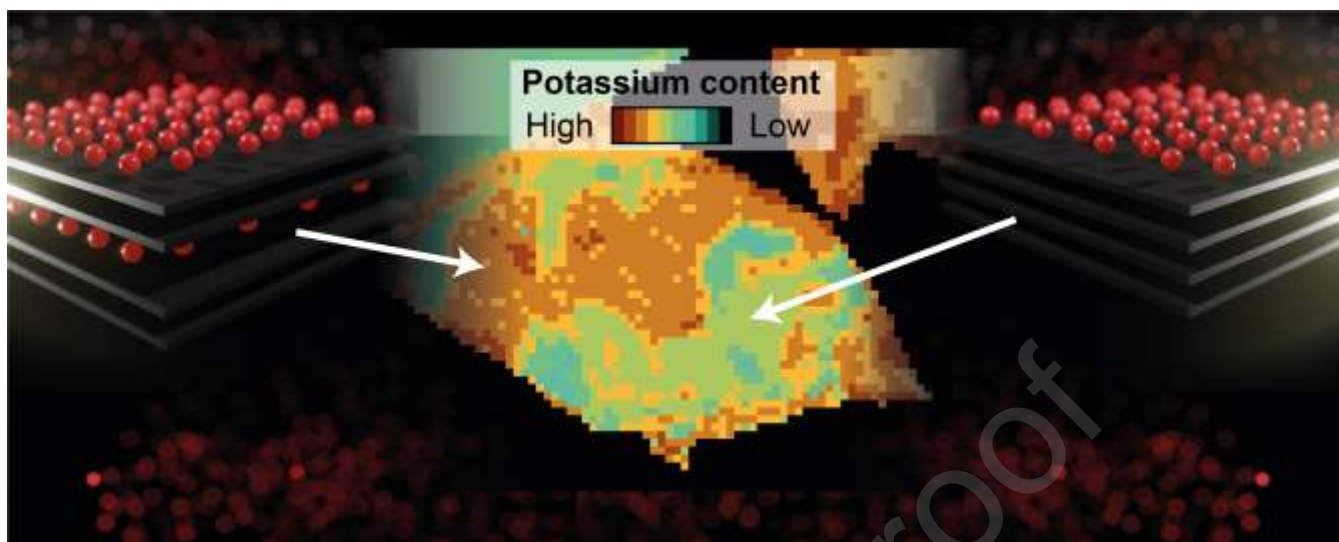
- [1] C. Schafhaeuti, Ueber die Verbindungen des Kohlenstoffes mit Silicium, Eisen und anderen Metallen, welche die verschiedenen Gallungen von Roheisen, Stahl und Schmiedeeisen bilden, *Journal für praktische Chemie* 21 (1840) 129-157. <https://doi.org/10.1002/prac.18400210117>.
- [2] Y. Li, Y. Lu, P. Adelhelm, M.-M. Titirici, Y.-S. Hu, Intercalation chemistry of graphite: alkali metal ions and beyond, *Chemical Society Reviews* 48 (2019) 4655-4687. <https://doi.org/10.1039/C9CS00162J>.
- [3] A. Lii-Rosales, Y. Han, D. Jing, M.C. Tringides, S. Julien, K.-T. Wan, C.-Z. Wang, K.C. Lai, J.W. Evans, P.A. Thiel, Encapsulation of metal nanoparticles at the surface of a prototypical layered material, *Nanoscale* 13 (2021) 1485-1506. <https://doi.org/10.1039/D0NR07024F>.
- [4] W. Li, L. Huang, M.C. Tringides, J.W. Evans, Y. Han, Thermodynamic preference for atom adsorption on versus intercalation into multilayer graphene, *The Journal of Physical Chemistry Letters* 11 (2020) 9725-9730. <https://doi.org/10.1021/acs.jpcllett.0c02887>.
- [5] M.S. Whittingham, Lithium batteries and cathode materials, *Chemical Reviews* 104 (2004) 4271-4301. <https://doi.org/10.1021/cr020731c>.
- [6] J. Xu, Y. Dou, Z. Wei, J. Ma, Y. Deng, Y. Li, H. Liu, S. Dou, Recent progress in graphite intercalation compounds for rechargeable metal (Li, Na, K, Al) - ion batteries, *Advanced Science* 4 (2017) 1700146. <https://doi.org/10.1002/advs.201700146>.
- [7] J.L. Miller, Lithium-ion battery pioneers awarded Chemistry Nobel, *Physics Today* 72 (2019) 20-24. <https://doi.org/10.1063/Pt.3.4359>.
- [8] W. Luo, J. Wan, B. Ozdemir, W. Bao, Y. Chen, J. Dai, H. Lin, Y. Xu, F. Gu, V. Barone, Potassium ion batteries with graphitic materials, *Nano letters* 15 (2015) 7671-7677. <https://doi.org/10.1021/acs.nanolett.5b03667>.
- [9] J. Zhang, T. Liu, X. Cheng, M. Xia, R. Zheng, N. Peng, H. Yu, M. Shui, J. Shu, Development status and future prospect of non-aqueous potassium ion batteries for large scale energy storage, *Nano Energy* 60 (2019) 340-361. <https://doi.org/10.1016/j.nanoen.2019.03.078>.
- [10] L. Fan, R. Ma, Q. Zhang, X. Jia, B. Lu, Graphite anode for a potassium - ion battery with unprecedented performance, *Angewandte Chemie* 131 (2019) 10610-10615. <https://doi.org/10.1002/anie.201904258>.
- [11] J.C. Chacón - Torres, L. Wirtz, T. Pichler, Raman spectroscopy of graphite intercalation compounds: Charge transfer, strain, and electron-phonon coupling in graphene layers, *physica status solidi (b)* 251 (2014) 2337-2355. <https://doi.org/10.1002/pssb.201451477>.
- [12] A.M. Dimiev, G. Ceriotti, N. Behabtu, D. Zakhidov, M. Pasquali, R. Saito, J.M. Tour, Direct real-time monitoring of stage transitions in graphite intercalation compounds, *ACS Nano* 7 (2013) 2773-2780. <https://doi.org/10.1021/nn400207e>.

- [13] W.Z. Bao, J.Y. Wan, X.G. Han, X.H. Cai, H.L. Zhu, D.H. Kim, D.K. Ma, Y.L. Xu, J.N. Munday, H.D. Drew, M.S. Fuhrer, L.B. Hu, Approaching the limits of transparency and conductivity in graphitic materials through lithium intercalation, *Nature Communications* 5 (2014) 4224. <https://doi.org/10.1038/ncomms5224>.
- [14] Y. Guo, R.B. Smith, Z. Yu, D.K. Efetov, J. Wang, P. Kim, M.Z. Bazant, L.E. Brus, Li intercalation into graphite: direct optical imaging and Cahn–Hilliard reaction dynamics, *The journal of physical chemistry letters* 7 (2016) 2151-2156. <https://doi.org/10.1021/acs.jpcclett.6b00625>.
- [15] E.R. White, J.J. Lodicio, B.C. Regan, Intercalation events visualized in single microcrystals of graphite, *Nature communications* 8 (2017) 1969. <https://doi.org/10.1038/s41467-017-01787-8>.
- [16] M. Kühne, F. Börnert, S. Fecher, M. Ghorbani-Asl, J. Biskupek, D. Samuelis, A.V. Krashennikov, U. Kaiser, J.H. Smet, Reversible superdense ordering of lithium between two graphene sheets, *Nature* 564 (2018) 234-239. <https://doi.org/10.1038/s41586-018-0754-2>.
- [17] S. Leung, M. Dresselhaus, C. Underhill, T. Krapchev, G. Dresselhaus, B. Wuensch, Structural studies of graphite intercalation compounds using (0 0 l) x-ray diffraction, *Physical Review B* 24 (1981) 3505. <https://doi.org/10.1103/PhysRevB.24.3505>.
- [18] N. Dumas, A. Hérold, Notes des Membres et Correspondants et Notes Présentée sou Transmises par Leurs Soins, *CR Acad. Sci. Ser. C* 268 (1969) 373-375.
- [19] K.S. Novoselov, A.K. Geim, S.V. Morozov, D. Jiang, Y. Zhang, S.V. Dubonos, I.V. Grigorieva, A.A. Firsov, Electric field effect in atomically thin carbon films, *Science* 306 (2004) 666-669. <https://doi.org/10.1126/science.1102896>.
- [20] K.S. Novoselov, A.K. Geim, S.V. Morozov, D. Jiang, M.I. Katsnelson, I.V. Grigorieva, S. Dubonos, Firsov, AA, Two-dimensional gas of massless Dirac fermions in graphene, *nature* 438 (2005) 197-200. <https://doi.org/10.1038/nature04233>.
- [21] C. Howard, M. Dean, F. Withers, Phonons in potassium-doped graphene: The effects of electron-phonon interactions, dimensionality, and adatom ordering, *Physical Review B* 84 (2011) 241404. <https://doi.org/10.1103/PhysRevB.84.241404>.
- [22] D. Marchiani, A. Tonelli, C. Mariani, R. Frisenda, J. Avila, P. Dudin, S. Jeong, Y. Ito, F.S. Magnani, R. Biagi, Tuning the Electronic Response of Metallic Graphene by Potassium Doping, *Nano Letters* 23 (2022) 170-176. <https://doi.org/10.1021/acs.nanolett.2c03891>.
- [23] D. Marchiani, R. Frisenda, C. Mariani, M. Sbroscia, T. Caruso, O. De Luca, M. Papagno, D. Pacilé, S. Jeong, Y. Ito, Charge Effects and Electron Phonon Coupling in Potassium-Doped Graphene, *ACS omega* 9 (2024) 39546-39553. <https://doi.org/10.1021/acsomega.4c03543>.
- [24] M. Lorenzo, C. Escher, T. Latychevskaia, H.-W. Fink, Metal adsorption and nucleation on free-standing graphene by low-energy electron point source microscopy, *Nano letters* 18 (2018) 3421-3427. <https://doi.org/10.1021/acs.nanolett.8b00359>.
- [25] R. Raccichini, A. Varzi, S. Passerini, B. Scrosati, The role of graphene for electrochemical energy storage, *Nature materials* 14 (2015) 271-279. <https://doi.org/10.1038/nmat4170>.
- [26] J. Hassoun, F. Bonaccorso, M. Agostini, M. Angelucci, M.G. Betti, R. Cingolani, M. Gemmi, C. Mariani, S. Panero, V. Pellegrini, An advanced lithium-ion battery based on a graphene anode and a lithium iron phosphate cathode, *Nano letters* 14 (2014) 4901-4906. <https://doi.org/10.1021/nl502429m>.
- [27] C. Zhong, S. Weng, Z. Wang, C. Zhan, X. Wang, Kinetic limits and enhancement of graphite anode for fast-charging lithium-ion batteries, *Nano Energy* (2023) 108894. <https://doi.org/10.1016/j.nanoen.2023.108894>.
- [28] E. Olsson, G. Chai, M. Dove, Q. Cai, Adsorption and migration of alkali metals (Li, Na, and K) on pristine and defective graphene surfaces, *Nanoscale* 11 (2019) 5274-5284. <https://doi.org/10.1039/C8NR10383F>.
- [29] X. Jiang, B. Song, D. Tománek, Formation Dynamics of Potassium-Based Graphite Intercalation Compounds: An Ab Initio Study, *Physical Review Applied* 9 (2018) 044015. <https://doi.org/10.1103/PhysRevApplied.9.044015>.
- [30] A. Castellanos-Gomez, M. Buscema, R. Molenaar, V. Singh, L. Janssen, H.S. Van Der Zant, G.A. Steele, Deterministic transfer of two-dimensional materials by all-dry viscoelastic stamping, *2D Materials* 1 (2014) 011002. <https://doi.org/10.1088/2053-1583/1/1/011002>.
- [31] Q. Zhao, T. Wang, Y.K. Ryu, R. Frisenda, A. Castellanos-Gomez, An inexpensive system for the deterministic transfer of 2D materials, *Journal of Physics: Materials* 3 (2020) 016001. <https://doi.org/10.1088/2515-7639/ab6a72>.
- [32] R.R. Nair, P. Blake, A.N. Grigorenko, K.S. Novoselov, T.J. Booth, T. Stauber, N.M. Peres, A.K. Geim, Fine structure constant defines visual transparency of graphene, *science* 320 (2008) 1308-1308. <https://doi.org/10.1126/science.1156965>.
- [33] Y. Liu, Z. Liu, W.S. Lew, Q.J. Wang, Temperature dependence of the electrical transport properties in few-layer graphene interconnects, *Nanoscale research letters* 8 (2013) 1-7. <https://doi.org/10.1186/1556-276X-8-335>.
- [34] L.M. Malard, M.A. Pimenta, G. Dresselhaus, M.S. Dresselhaus, Raman spectroscopy in graphene, *Physics reports* 473 (2009) 51-87. <https://doi.org/10.1016/j.physrep.2009.02.003>.
- [35] Y. Wang, Z. Ni, Z. Shen, H. Wang, Y. Wu, Interference enhancement of Raman signal of graphene, *Applied Physics Letters* 92 (2008) <https://doi.org/10.1063/1.2838745>.
- [36] S.-L. Li, H. Miyazaki, H. Song, H. Kuramochi, S. Nakaharai, K. Tsukagoshi, Quantitative Raman spectrum and reliable thickness identification for atomic layers on insulating substrates, *ACS nano* 6 (2012) 7381-7388. <https://doi.org/10.1021/nn3025173>.
- [37] J.E. Lee, G. Ahn, J. Shim, Y.S. Lee, S. Ryu, Optical separation of mechanical strain from charge doping in graphene, *Nature communications* 3 (2012) 1024. <https://doi.org/10.1038/ncomms2022>.
- [38] P. Szirmai, B.G. Márkus, J.C. Chacón-Torres, P. Eckerlein, K. Edlthammer, J.M. Englert, U. Mundloch, A. Hirsch, F. Hauke, B. Náfrádi, Characterizing the maximum number of layers in chemically exfoliated graphene, *Scientific reports* 9 (2019) 19480. <https://doi.org/10.1038/s41598-019-55784-6>.
- [39] K. Share, A.P. Cohn, R.E. Carter, C.L. Pint, Mechanism of potassium ion intercalation staging in few layered graphene from in situ Raman spectroscopy, *Nanoscale* 8 (2016) 16435-16439. <https://doi.org/10.1039/c6nr04084e>.
- [40] K. Ji, J. Han, A. Hirata, T. Fujita, Y. Shen, S. Ning, P. Liu, H. Kashani, Y. Tian, Y. Ito, Lithium intercalation into bilayer graphene, *Nature communications* 10 (2019) 275. <https://doi.org/10.1038/s41467-018-07942-z>.
- [41] T. Astles, J.G. McHugh, R. Zhang, Q. Guo, M. Howe, Z. Wu, K. Indykiewicz, A. Summerfield, Z.A. Goodwin, S. Slizovskiy, In-plane staging in lithium-ion intercalation of bilayer graphene, *Nature Communications* 15 (2024) 6933. <https://doi.org/10.1038/s41467-024-51196-x>.

- [42] J. Yan, Y. Zhang, P. Kim, A. Pinczuk, Electric field effect tuning of electron-phonon coupling in graphene, *Physical review letters* 98 (2007) 166802. <https://doi.org/10.1103/PhysRevLett.98.166802>.
- [43] A. Das, S. Pisana, B. Chakraborty, S. Piscanec, S.K. Saha, U.V. Waghmare, K.S. Novoselov, H.R. Krishnamurthy, A.K. Geim, A.C. Ferrari, Monitoring dopants by Raman scattering in an electrochemically top-gated graphene transistor, *Nature nanotechnology* 3 (2008) 210-215. <https://doi.org/10.1038/nnano.2008.67>.
- [44] M. Freitag, M. Steiner, Y. Martin, V. Perebeinos, Z. Chen, J.C. Tsang, P. Avouris, Energy dissipation in graphene field-effect transistors, *Nano letters* 9 (2009) 1883-1888. <https://doi.org/10.1021/nl803883h>.
- [45] J. Sonntag, K. Watanabe, T. Taniguchi, B. Beschoten, C. Stampfer, Charge carrier density dependent Raman spectra of graphene encapsulated in hexagonal boron nitride, *Physical Review B* 107 (2023) 075420. <https://doi.org/10.1103/PhysRevB.107.075420>.
- [46] S. Pisana, M. Lazzeri, C. Casiraghi, K.S. Novoselov, A.K. Geim, A.C. Ferrari, F. Mauri, Breakdown of the adiabatic Born–Oppenheimer approximation in graphene, *Nature materials* 6 (2007) 198-201. <https://doi.org/10.1038/nmat1846>.
- [47] D. Basko, S. Piscanec, A. Ferrari, Electron-electron interactions and doping dependence of the two-phonon Raman intensity in graphene, *Physical Review B* 80 (2009) 165413. <https://doi.org/10.1103/PhysRevB.80.165413>.
- [48] C. Casiraghi, Raman intensity of graphene, *physica status solidi (b)* 248 (2011) 2593-2597. <https://doi.org/10.1002/pssb.201100040>.
- [49] Y.-C. Lin, R. Matsumoto, Q. Liu, P. Solís-Fernández, M.-D. Siao, P.-W. Chiu, H. Ago, K. Suenaga, Alkali metal bilayer intercalation in graphene, *Nature communications* 15 (2024) 425. <https://doi.org/10.1038/s41467-023-44602-3>.
- [50] Y. Han, A. Lii-Rosales, M.C. Tringides, J.W. Evans, P.A. Thiel, Energetics of Cu adsorption and intercalation at graphite step edges, *Physical Review B* 99 (2019) 115415. <https://doi.org/10.1103/PhysRevB.99.115415>.
- [51] J. Zhang, A. Yang, X. Wu, J. van de Groep, P. Tang, S. Li, B. Liu, F. Shi, J. Wan, Q. Li, Reversible and selective ion intercalation through the top surface of few-layer MoS₂, *Nature communications* 9 (2018) 5289. <https://doi.org/10.1038/s41467-018-07710-z>.
- [52] E.M. Gavilán-Arriazu, O.A. Pinto, B.L. de Mishima, D. Barraco, O.A. Oviedo, E.P.M. Leiva, The kinetic origin of the Daumas-Hérolld model for the Li-ion/graphite intercalation system, *Electrochemistry Communications* 93 (2018) 133-137. <https://doi.org/10.1016/j.elecom.2018.07.004>.
- [53] H. Park, D.S. Wragg, A.Y. Kuposov, Replica exchange molecular dynamics for Li-intercalation in graphite: a new solution for an old problem, *Chemical Science* 15 (2024) 2745-2754. <https://doi.org/10.1039/D3SC06107H>.
- [54] F. Ding, H. Ji, Y. Chen, A. Herklotz, K. Dörr, Y. Mei, A. Rastelli, O.G. Schmidt, Stretchable graphene: a close look at fundamental parameters through biaxial straining, *Nano letters* 10 (2010) 3453-3458. <https://doi.org/10.1021/nl101533x>.
- [55] J. Zabel, R.R. Nair, A. Ott, T. Georgiou, A.K. Geim, K.S. Novoselov, C. Casiraghi, Raman spectroscopy of graphene and bilayer under biaxial strain: bubbles and balloons, *Nano letters* 12 (2012) 617-621. <https://doi.org/10.1021/nl203359n>.
- [56] S. Weng, S. Wu, Z. Liu, G. Yang, X. Liu, X. Zhang, C. Zhang, Q. Liu, Y. Huang, Y. Li, Localized - domains staging structure and evolution in lithiated graphite, *Carbon Energy* 5 (2023) e224.
- [57] J.C. Chacon-Torres, L. Wirtz, T. Pichler, Manifestation of charged and strained graphene layers in the Raman response of graphite intercalation compounds, *ACS nano* 7 (2013) 9249-9259. <https://doi.org/10.1021/nn403885k>.
- [58] M. Lazzeri, A.M. Saitta, F. Mauri, Breakdown of the adiabatic approximation in a doped graphene monolayer and in metallic carbon nanotubes, *physica status solidi (b)* 244 (2007) 4118-4123. <https://doi.org/10.1002/pssb.200776106>.
- [59] M. Lazzeri, F. Mauri, Nonadiabatic Kohn anomaly in a doped graphene monolayer, *Physical review letters* 97 (2006) 266407. <https://doi.org/10.1103/PhysRevLett.97.266407>.
- [60] D. Nixon, G. Parry, The expansion of the carbon-carbon bond length in potassium graphites, *Journal of Physics C: Solid State Physics* 2 (1969) 1732. <https://doi.org/10.1088/0022-3719/2/10/305>.
- [61] I.V. Chepkasov, M. Ghorbani-Asl, Z.I. Popov, J.H. Smet, A.V. Krashennnikov, Alkali metals inside bi-layer graphene and MoS₂: Insights from first-principles calculations, *Nano Energy* 75 (2020) 104927. <https://doi.org/10.1016/j.nanoen.2020.104927>.
- [62] J.Y. Kwak, Absorption coefficient estimation of thin MoS₂ film using attenuation of silicon substrate Raman signal, *Results in Physics* 13 (2019) 102202. <https://doi.org/10.1016/j.rinp.2019.102202>.
- [63] P. Giannozzi, S. Baroni, N. Bonini, M. Calandra, R. Car, C. Cavazzoni, D. Ceresoli, G.L. Chiarotti, M. Cococcioni, I. Dabo, QUANTUM ESPRESSO: a modular and open-source software project for quantum simulations of materials, *Journal of physics: Condensed matter* 21 (2009) 395502. <https://doi.org/10.1088/0953-8984/21/39/395502>.
- [64] P. Giannozzi, O. Andreussi, T. Brumme, O. Bunau, M.B. Nardelli, M. Calandra, R. Car, C. Cavazzoni, D. Ceresoli, M. Cococcioni, Advanced capabilities for materials modelling with Quantum ESPRESSO, *Journal of physics: Condensed matter* 29 (2017) 465901. <https://doi.org/10.1088/1361-648X/aa8f79>.
- [65] D. Hamann, Optimized norm-conserving Vanderbilt pseudopotentials, *Physical Review B—Condensed Matter and Materials Physics* 88 (2013) 085117. <https://doi.org/10.1103/PhysRevB.88.085117>.

Declaration of Competing Interest

The authors declare that they have no known competing financial interests or personal relationships that could have appeared to influence the work reported in this paper.



Highlights

- Spatially resolved Raman spectroscopy in ultra-high vacuum to unveil the dynamics of potassium adsorption, diffusion, and intercalation in few-layer graphene.
- The potassium diffusion in few-layer graphene is a collective and complex phenomenon due to varying energy barriers for the diffusion of adsorbed versus intercalated atoms.
- Charging, strain and layer decoupling in few-layer graphene are assessed.
- Density functional theory calculations show that both charging and steric hindrance introduce local strain in the graphene layers.